THE JOURNAL OF PHYSICAL CHEMISTRY A

ARTICLE

pubs.acs.org/JPCA

Polarization Modulation Spectroscopy of Single Fluorescent Nanodiamonds with Multiple Nitrogen Vacancy Centers

Yuen Yung Hui,*[,†] Yi-Ren Chang,[†] Nitin Mohan,[†] Tsong-Shin Lim,[‡] Yi-Ying Chen,[†] and Huan-Cheng Chang*[,†]

[†]Institute of Atomic and Molecular Sciences, Academia Sinica, Taipei 106, Taiwan

[‡]Department of Physics, Tunghai University, Taichung 407, Taiwan

Supporting Information

ABSTRACT: A technique based on polarization modulation spectroscopy (PMS) has been developed to determine quantitatively the number of fluorophores in nanoparticles at the single-molecule level. The technique involves rotation of the polarization of the excitation laser on a millisecond time scale, leading to fluorescence intensity modulation. By taking account of the heterogeneous orientation among the dipoles of the fluorophores and simulating the modulation depth distribution with Monte Carlo calculations, we show that it is possible to deduce the ensemble average and number distribution of the fluorophores. We apply the technique to fluorescent nanodiamonds (FNDs) containing multiple nitrogen vacancy (NV) centers. Comparing the experimental and simulated modulation depth distributions of 11 nm FNDs, we deduce an average number of $\langle N \rangle = 3$, which is in good agreement with independent photon correlation measurements. The method is general, rapid, and applicable to other nanoparticles, polymers, and molecular complexes containing multiple and randomly orientated fluorophores as well.

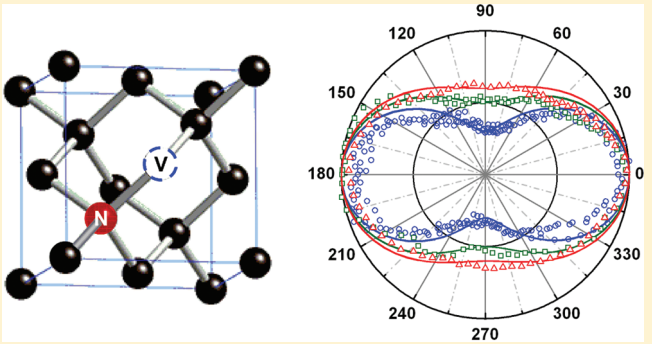

INTRODUCTION

Photon correlation spectroscopy (PCS) has been widely applicable to quantify the number of fluorophores in macromolecules and nanoparticles.[1−3] However, the quantification for multiple fluorophores is often complicated and hampered by the heterogeneous orientation of the fluorophore's dipole moments with respect to the polarization of the incident light.[4−6] As a result, the observed antibunching dip does not reflect directly the actual number of the dipoles within the same particle. The deviation becomes more pronounced as the number of the fluorophores increases. In a previous study,[6] we proposed to circumvent this problem by exciting the same nanoparticles of interest with both linearly and circularly polarized lights, observing the antibunching dips at the two different polarizations, and obtaining the histogram of the effective numbers of the fluorophores in the individual particles. By taking account of the heterogeneous orientation among the dipoles and simulating the probability distribution of the effective numbers with Monte Carlo calculations, we can deduce the actual number of these fluorophores in each nanoparticle. The method was illustrated with the fluorophore containing one dipole.[6]

A drawback of PCS is that it usually demands 10^6-10^7 photons in the measurement,[6] which is feasible only if photobleaching-resistant molecules are investigated and/or photobleaching is significantly suppressed. The experiment is technically challenging. In this work, we offer an alternative, polarization modulation spectroscopy (PMS), that does not require fast electronics to estimate the number of randomly orientated fluorophores.[7−10] We have previously demonstrated that the conformation of fluorescent polymers can be determined by PMS.[11−13] This is because the depth of the fluorescence intensity modulation is sensitive to the dipole orientation distribution of the fluorophores in the polymers.[13] It suggests that the technique may be applicable to measure rapidly the average number of the fluorophores in individual nanoparticles, if the heterogeneity in dipole orientation is properly taken into account and the probability distribution of the effective fluorophore numbers is adequately simulated with Monte Carlo calculations.

Here, we apply PMS plus Monte Carlo simulation to characterize the average number of fluorescent centers in nanodiamonds[14−16] because the nanomaterial holds great potential applications in biology.[17,18] It is biocompatible and nontoxic, and its surface can be easily derivatized with a variety of organic functionalized groups. Additionally, the negatively charged nitrogen vacancy (NV^-) centers in the fluorescent nanodiamond (FND) can emit far-red fluorescence, well-suited for bioimaging application.[19−22] The NV^- center in diamond is a point defect consisting of a substitutional nitrogen atom adjacent to a carbon

Received: November 10, 2010
Revised: December 24, 2010
Published: February 20, 2011

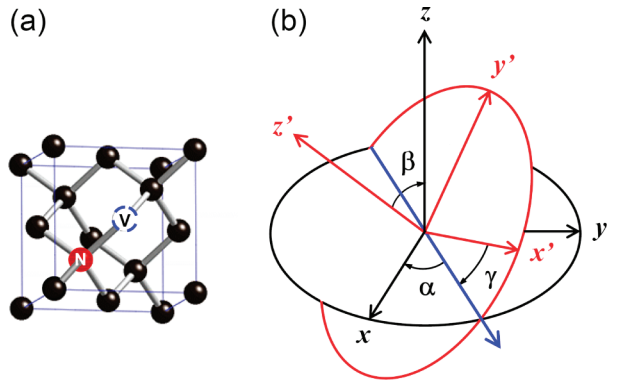

Figure 1. (a) Structure of an N—V center in diamond. The carbon atoms, nitrogen atom, and vacancy are denoted by black spheres, a dark red sphere, and a blue dashed circle, respectively. (b) Euler angles used to describe the spatial orientation of two degenerate orthogonal dipoles. The fixed coordinate system (in black) is denoted as (x,y,z), and the rotated coordinate system (in red) is denoted as (x',y',z'). The line of nodes is in blue. For simplicity, the unit vectors of the two orthogonal dipoles are defined as $\hat{\mathbf{p}}_1 = (1,0,0)$ and $\hat{\mathbf{p}}_2 = (0,1,0)$ in the (x',y',z') reference frame, and the polarization of the linearly polarized light before rotation is defined as $\hat{\mathbf{E}} = (1,0,0)$ in the (x,y,z) reference frame.

atom vacancy with C_{3v} symmetry (cf. Figure 1a).[23,24] It exhibits an optical absorption band at 1.945 eV (or 638 nm), accompanied by a broad phonon side band peaking at ~2.2 eV.[25] Strain dependence measurements indicated that the optical transition arises from the ^{3}A ground state to the ^{3}E electronically excited state.[25] The transition is allowed for two degenerate dipoles, which are orthogonal to each other, lying in the plane perpendicular to the symmetry axis.[24,26] Radiative relaxation of the excited state has a very high quantum efficiency, close to 1.[27] Moreover, the fluorescence is perfectly stable with neither photoblinking nor photobleaching. The combination of these outstanding features has enabled the detection of a single NV^- center in bulk diamond at room temperature[28] and has stimulated a wide range of applications including a single-photon source,[29] quantum information and computation,[30] high-resolution magnetometry,[31,32] super-resolution far-field optical microscopy,[33] and bioimaging[22] using the NV^- centers.

In this work, FNDs are excited by linearly polarized light, whose polarization is periodically rotated on a millisecond time scale.[11,13] As a result of the angles between the polarization of the laser and the dipole orientation of the individual NV centers being regulated periodically at the modulation frequency, the fluorescence intensity of the nanoparticle is modulated periodically.[14] From an analysis of the fluorescence modulation depth and a comparison of it with Monte Carlo simulation, we have been able to estimate the average number of NV centers in each FND particle. Our results show good agreement with the experimental data obtained by PCS.

SIMULATION AND RESULT

We present in this section a theoretical modeling for both PCS and PMS of single nanoparticles, each of which contains multiple and heterogeneously oriented fluorophores. We focus our discussion on the case that the fluorophore has two degenerate orthogonal dipoles associated with the transition between the ground and excited states. The treatment can be similarly applied to analyze a one-dipole case.[6]

We start the modeling with PCS, which has been widely used to quantify the number of NV^- centers in the FND particle.[4−6] We consider the second-order correlation function of the fluorescence signal[1,2]

$$g^{(2)}(\tau) = \langle I(t)I(t+\tau)\rangle/\langle I(t)\rangle^2 \quad (1)$$

where τ is the interphoton time, $I(t)$ is the fluorescence intensity at the time t, and the bracket denotes the average over the detection time interval. In a system with N independent and identical emitters, eq 1 can be rewritten as[1]

$$g^{(2)}(\tau) = 1 - e^{-k_d|\tau|}/N \quad (2)$$

where k_d is the decay rate of the spontaneous emission in a pure two-level system and the decay rate is larger than the excitation rate. When the intensities of the fluorescence from the individual fluorophores are not identical, the second-order correlation function can be approximated in a more general form as (see Supporting Information for details)[2]

$$g^{(2)}(\tau) = 1 - \left[\frac{\sum_{j=1}^{N} I^2_j}{(\sum_{j=1}^{N} I_j)^2}\right] e^{-k_d|\tau|} \quad (3)$$

where I_j is the average fluorescence intensity of the jth fluorophore, which is proportional to its absorption rate. Hence, the effective (or measured) number, N_e, for the heterogeneously oriented emission centers is given as

$$N_e = (\sum_{j=1}^{N} I_j)^2 / \sum_{j=1}^{N} I^2_j \quad (4)$$

As for PMS, the parameter of interest is the fluorescence modulation depth, which is defined as[11]

$$M = (I_{max} - I_{min})/(I_{max} + I_{min}) \quad (5)$$

where I_{max} and I_{min} are the maximum and minimum values of the modulated fluorescence intensity, $I_m(t)$, respectively. In treating particles containing multiple fluorophores, the equation should be generalized to

$$M = \frac{(\sum_{j=1}^{N} I_j)_{max} - (\sum_{j=1}^{N} I_j)_{min}}{(\sum_{j=1}^{N} I_j)_{max} + (\sum_{j=1}^{N} I_j)_{min}} \quad (6)$$

To calculate explicitly the fluorescence intensity I_j for each fluorophore with two degenerate orthogonal dipoles in the transition, we consider these dipoles to lie in the $x'-y'$ plane of the rotating reference frame (x',y',z'), as illustrated in Figure 1b. They can be expressed as $\hat{\mathbf{p}}_1 = (1,0,0)$ and $\hat{\mathbf{p}}_2 = (0,1,0)$, respectively. Using Euler angles as defined in the figure, it is easy to show that the unit vectors of these two dipoles in the laboratory reference frame (x,y,z) have the forms[34,35]

$$\hat{\mathbf{p}}_1 = \begin{pmatrix} \cos\alpha\cos\gamma - \sin\alpha\cos\beta\sin\gamma \\ \sin\alpha\cos\gamma + \cos\alpha\cos\beta\sin\gamma \\ \sin\beta\sin\gamma \end{pmatrix} \quad (7)$$

and

$$\hat{\mathbf{p}}_2 = \begin{pmatrix} -\cos\alpha\sin\gamma - \sin\alpha\cos\beta\cos\gamma \\ -\sin\alpha\sin\gamma + \cos\alpha\cos\beta\cos\gamma \\ \sin\beta\cos\gamma \end{pmatrix} \quad (8)$$

where we drop the subscripts j in the equations here and hereafter for simplicity. In the cases that the polarization of the excitation laser beam sits in the $x-y$ plane,[6] the electric field of the linearly polarized light can be written as $\hat{\mathbf{E}} = (\cos\varphi_e, \sin\varphi_e, 0)$, where φ_e is the angle between $\hat{\mathbf{E}}$ and the x axis. Setting $\varphi_e = 0$ for convenience in the following treatment, one can show readily that the time-average fluorescence intensity (I_l) of the individual fluorophores excited by the linearly polarized light is

$$I_l \propto \langle \sum_i^2 (\hat{\mathbf{p}}_i \cdot \hat{\mathbf{E}})^2 \rangle \propto 1 - \sin^2\alpha \cdot \sin^2\beta \quad (9)$$

and the corresponding fluorescence intensity (I_c) due to excitation by the circularly polarized light is then

$$I_c \propto \langle \sum_i^2 (\hat{\mathbf{p}}_i \cdot \hat{\mathbf{E}})^2 \rangle \propto 1 + \cos^2\beta \quad (10)$$

Applying the same treatment to PMS, we consider the polarization of the light modulated with a frequency of ω_m as $\hat{\mathbf{E}}_m = (\cos\omega_m t, \sin\omega_m t, 0)$.[11] The resultant fluorescence intensity of the individual fluorophore can be derived as

$$I_m(t) \propto \sum_i^2 (\hat{\mathbf{p}}_i \cdot \hat{\mathbf{E}})^2 \propto 1 - \sin^2(\alpha - \omega_m t) \cdot \sin^2\beta \propto [6 + 2\cos 2\beta + 2\cos 2(\alpha - \omega_m t) - \cos 2(\alpha + \beta - \omega_m t) - \cos 2(\alpha - \beta - \omega_m t)]/8 \quad (11)$$

which predicts that the fluorescence intensity will oscillate at a frequency of $2\omega_m$. Furthermore, it predicts that the fluorescence intensity will depend only on the Euler angles α and β but not on γ which lies in the $x'-y'$ plane defined by the two orthogonal dipoles of the same magnitude.[24] In general, the angle α determines the phase of the modulated intensity, and the angle β determines the modulation depth. Figure 2 shows some simulated results at $\beta = 0°$, ($\alpha = 180°, \beta = 45°$), and ($\alpha = 0°, \beta = 90°$). In the case of FND, according to eq 11, the fluorescence intensity of a single NV^- center will vary with the trajectory of the projected image of the two orthogonal dipoles on the $x-y$ plane. If the C_{3v} axis of the NV^- center is parallel to the propagating direction of the laser beam (along the z-direction), both of the orthogonal dipoles are exactly perpendicular to the z-direction (hence, $\beta = 0°$). The projection of these two degenerate orthogonal dipoles on the $x-y$ plane is a circle; hence, the fluorescence intensity is a constant. No modulation will be seen.[26] By contrast, if the C_{3v} axis is tilted with $\beta = 90°$, the modulation is 100%.

In applying the above formulas to multiple NV^- centers in FND, we employ Monte Carlo simulations to compute the effective number N_e according to eqs 4, 9, and 10 at various N. We assume that the crystal orientation of the spin-coated nanodiamonds is totally random on the cover glass. Also, the orientation of each NV^- center is assumed to be equally probable in the nanocrystal, which is a good approximation in the bulk crystal.[24,26] Due to the symmetry of the diamond lattice, each

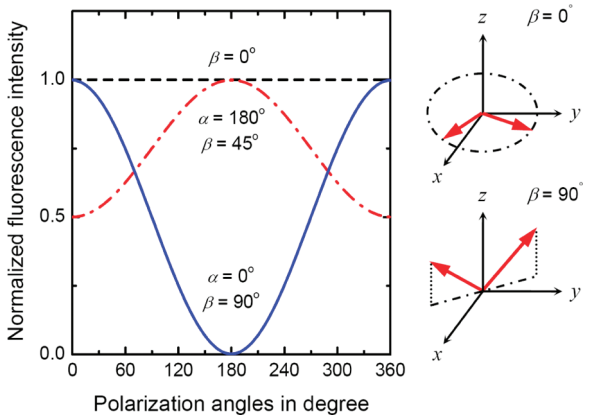

Figure 2. Dependence of fluorescence intensity on the orientation of the fluorophore with two degenerate orthogonal dipoles. Insets (right): The thick red arrow represents the orthogonal dipoles. During the polarization modulation experiment, the polarization of the laser beam is rotating in the $x-y$ plane. Hence, the resultant fluorescence intensity, $\sum_i^2 (\hat{\mathbf{p}}_i \cdot \hat{\mathbf{E}})^2$, is determined by the projection of the dipole moment $\hat{\mathbf{p}}_i$ on this plane with respect to $\hat{\mathbf{E}}$. As $\beta = 0°$ (defined in Figure 1b), both dipole moments lie in the $x-y$ plane, and the projection travels along the dashed circle because the polarization of the laser beam is rotating during experiment. The fluorescence intensity is a constant. As $\beta = 90°$, the projection travels along the dashed straight line passing through the origin. The fluorescence intensity varies along the dashed line.

NV^- center can have only four possible configurations in the crystal matrix (Figure 1a).[36] Therefore, to simulate all possible orientations of these NV^- centers, we set the orientation of the first NV^- center to be random in space by the Monte Carlo method, but the orientation of the next NV^- center in the same particle is restricted to one of the four equally probable configurations. Once the orientations of these NV^- centers in the same FND particle are chosen, the effective number N_e of the fluorophores is computed at a given N.

Figure 3a and b shows the simulated probability distributions of N_e with 10 000 particles measured in either circular or linear polarization, denoted by $N_{e,c}$ and $N_{e,l}$, respectively. As seen, the average number of $N_{e,l}$ is always smaller than the corresponding $N_{e,c}$ for each N. In Figure 3c, we plot the correlation between the average effective number $\langle N_e \rangle$ and the actual number N, with the error bar indicating the standard deviation of the simulated probability distribution. Both of the average effective numbers, $\langle N_{e,l} \rangle$ and $\langle N_{e,c} \rangle$, under linearly and circularly polarized excitations are linearly proportional to N in a form of $N - 1 = 1.2 \cdot (\langle N_{e,l} \rangle - 1)$ and $N - 1 = \langle N_{e,c} \rangle - 1$, respectively. In particular, the average effective number under the circular excitation is essentially the same as the actual number when $N < 10$. In our previous work,[6] we studied the number of NV^- centers for 28 nm FNDs prepared by 3-MeV proton irradiation using PCS. We then applied a single dipole instead of two orthogonal dipoles during Monte Carlo simulation and estimated the average number ($\langle N \rangle$) of NV^- centers in these particles as 7. Referring to Figure 3c, the actual numbers deduced by linearly and circularly polarized light are $\langle N \rangle = 5.8$ and 6.3, respectively. Hence, such 28 nm FND should contain 6 ± 1 centers per particle.

In PMS, the polarization of the excitation laser beam is rotating, and hence, the resultant fluorescence intensity can vary periodically. For NV^- in FND, each center in the same particle contributes not only to the total fluorescence intensity but also to

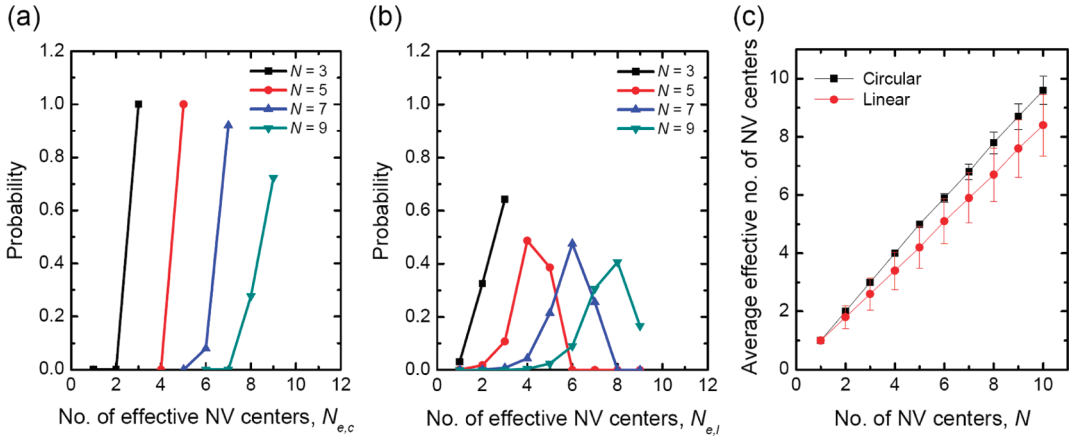

Figure 3. (a, b) Simulated histograms for the effective numbers of NV centers in single FND particles excited by (a) circularly polarized light and (b) linearly polarized light. N is the actual number of the NV centers. (c) Relationship between the average effective number, $\langle N_e \rangle$, and the actual number, N, of NV centers in FND excited by linearly and circularly polarized lights. The error bar denotes the standard deviation of the simulated distribution in (a) and (b).

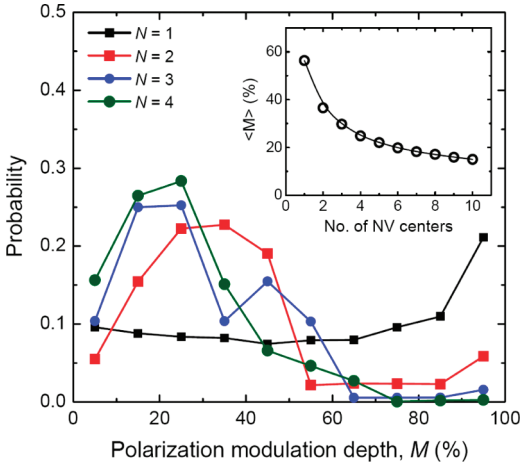

Figure 4. Simulated modulation depth histograms of FND fluorescence by polarization modulation spectroscopy, where N is the number of NV centers. Each data point on the x-axis represents the midpoint of a calculated range of 10%. The curve in the inset shows the relationship between the average modulation depth and the number of NV centers.

the modulation depth M. With Monte Carlo simulation, we calculate specifically the probability distributions of M at various N based on eqs 6 and 11. As shown in Figure 4, the distributions exhibit distinctly different patterns at $N \leq 4$. We can easily distinguish particles containing a single NV center from particles containing multiple centers by the modulation depth histograms. Moreover, the average modulation depth $\langle M \rangle$ depends sensitively on the number of the fluorophores (inset in Figure 4). It decreases sharply at $N \leq 4$ and gradually levels off at increasing N. Both results indicate that the number of NV^- centers in FND can be deduced from PMS when N is small.

EXPERIMENT AND RESULT

Experimentally, we quantified the number of NV centers in FND particles with a mean size of 11 nm.[37,38] A complication, unfortunately, arises in the quantification, that is, the NV centers in 11 nm FNDs can exist in two different forms, NV^- and NV^0.[39] The neutral NV center exhibits a zero-phonon line at 575 nm, and its photoluminescence band peaks at ~620 nm.[40] Previous strain-dependent measurements for NV^0 have shown that this center has a trigonal symmetry and its transition occurs between the ^2A excited state and the ^2E ground state.[41] The transition dipoles are doubly degenerate and orthogonal, the same as those of NV^-. Although there is a slight distortion of the symmetry due to the Jahn−Teller effect,[42] it can be ignored in the present treatment. Zheng et al.[16] have recently studied in detail the spectroscopic properties of NV^0. They found that the numbers of photons emitted from the negative and the neutral NV centers excited at 532 nm are comparable to each other at low excitation energies. According to a recent study on FNDs of a size of less than 8 nm,[43] the NV centers in these particles can retain their bulk fluorescence characteristics. We thereby approximate and simplify the following analysis without distinguishing these two types of NV centers.

We produced 11 nm FNDs by centrifugal extraction of a 35 nm FND ensemble, prepared by ion bombardment of type-Ib diamond powders (Microdiamant MSY 0-0.05) with 40 keV He^+ and subsequent annealing at 800 °C in vacuum. To remove graphitic surface structures, the freshly prepared FNDs were first oxidized in air at 450 °C, cleaned at 100 °C in strong oxidative acids, and finally rinsed extensively in water.[38] Photon correlation measurements, as detailed previously,[6,37] were conducted for FND particles spin-coated on a cover glass slide with a density of ~5 particles per 20 × 20 μm^2. A cw frequency-doubled Nd:YAG laser (DPGL-2100F; λ = 532 nm) was focused onto the specimen by an oil immersion objective (Nikon E600; 100×, NA = 1.3). A quarter waveplate was inserted in the optical path to switch the laser excitation from linear to circular polarization. The laser power was kept below 100 μW, far below the saturation power of the FND. The fluorescence was collected by the same microscope objective, filtered by a dichroic mirror (Omega 550DCLP) and an emission filter (Chroma D705/190M), and then focused onto two avalanche photodiodes (Perkin-Elmer SPCM-AQR-15-FC). The two photodiodes produced start and stop signals for a time-correlated single-photon counting system (PicoHarp 300). By measuring the temporal separation between these two detectors, we observed the antibunching dip and deduced the number of NV^- centers from the depth of the dip.

dx.doi.org/10.1021/jp110761u |J. Phys. Chem. A 2011, 115, 1878–1884

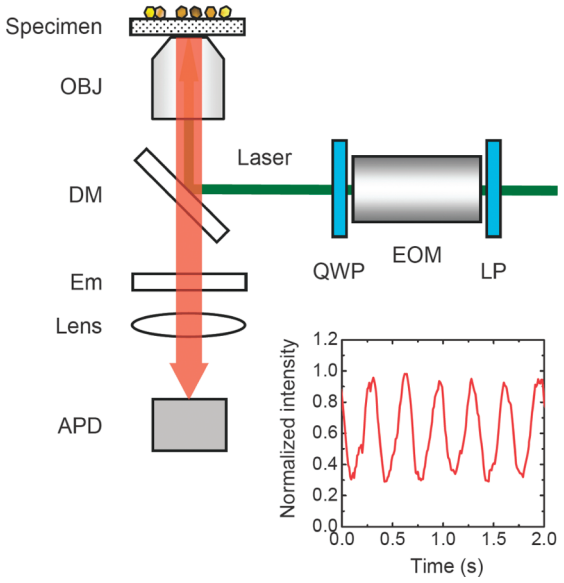

Figure 5. Experimental setup for polarization modulation spectroscopy. See text for details. APD: avalanche photodiode; DM: dichroic mirror; EM: emission filter, EOM: electro-optical modulator; LP: linear polarizer; OBJ: objective lens; QWP: quarter-wave plate. Inset (bottom): The corresponding fluorescence time trace for 11 nm FND particles during polarization modulation experiment. The time axis corresponds to the polarization angle of the excitation laser.

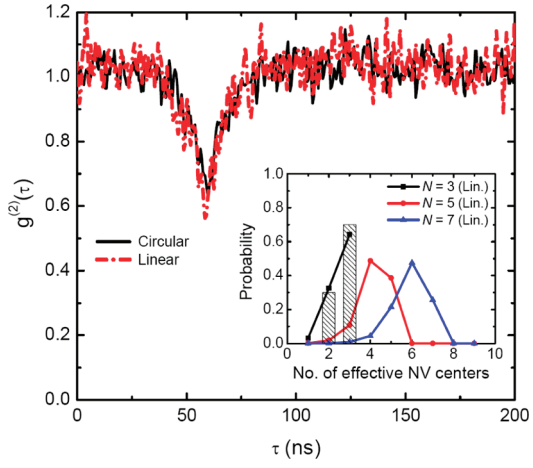

Figure 6. Typical photon correlation measurements for a single 11 nm FND particle at two different polarizations. The bar chart in the inset is the experimental data for effective number of the 11 nm FNDs measured by linearly polarized light. All of these FNDs contain three NV centers per particle as determined by circularly polarized light.

Meanwhile, PMS was conducted in the same microscope system. A schematic diagram of the experimental setup is shown in Figure 5.[11] To conduct the PMS measurements, a modulator regulated the polarization of the laser beam continuously. The modulator consisted of a linear polarizer, an electro-optical modulator (Conoptics 350−50), and a quarter waveplate, which rotated the polarization of the laser beam at a fixed frequency of ω_m = 1.5 Hz. The resulting fluorescence was directly collected to the avalanche photodiode. The inset of Figure 5 presents a typical fluorescence time trace, showing an oscillation frequency of 3.0 Hz.

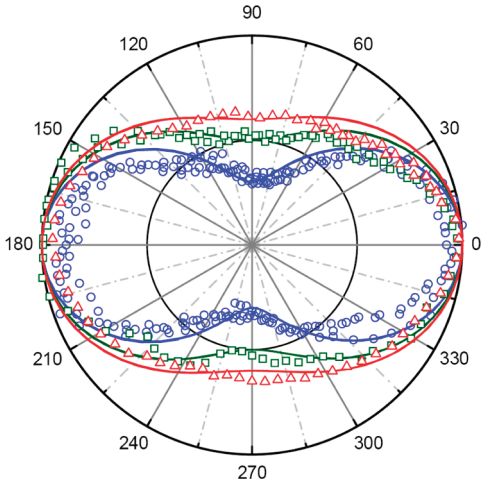

Figure 7. Normalized fluorescence intensities of NV centers as a function of the polarization (in angles) of the excitation laser for three different 11 nm FND particles. Solid curves are included to serve as a guide to the eye.

Our previous work has applied circularly polarized light for the photon correlation measurement and determined that the average number of NV centers in 11 nm FNDs is $\langle N \rangle = 3$.[37] Here, we check further the corresponding antibunching curves with both circularly and linearly polarized lights. Figure 6 shows the result of the measurement for an 11 nm FND. The actual number of the NV center in the particle is $N = 3$ as determined by PCS using circularly polarized light. However, the linearly polarized light infers two centers, as indicated in the same figure. Such a discrepancy is explained by the heterogeneous orientation among the NV centers. To make a statistically meaningful comparison, we employed circularly polarized light to identify 10 particles, each of which contains 3 NV centers, and measured the corresponding effective number of the centers with linearly polarized light. The experimental result is given in the inset of Figure 6, which confirms the simulation.

Following the PCS measurements, we applied PMS to the same 11 nm FND ensemble and recorded the modulation depths for 64 particles. Figure 7 presents the results of three particles, plotted in polar coordinates according to the fluorescence intensity versus the polarization of the light.[24] Each particle shows an anisotropic dumbbell-like pattern. One can derive the modulation depth from the difference between the long axis and the short axis of the dumbbell. The anisotropy of the pattern observed here depends not only on the relative orientation of the two orthogonal dipoles with respect to the polarization of the light (cf. Figure 2)[15] but also on the number of the NV centers in each particle. A histogram of the modulation depths collected for 64 particles is depicted in Figure 8, and the obtained average modulation depth is 27%. Comparing it with the Monte Carlo simulation as shown in the inset of the same figure for $\langle M \rangle$ suggests that there are, on average, three NV centers in each 11 nm FND particle. The result is in excellent agreement with the average number of $\langle N \rangle = 3 \pm 1$ deduced by PCS for the same ensemble of particles.[37] It is noted that the photoluminescence intensity of our 11 nm FND with three NV centers is comparable with that of single red quantum dots at saturation of their excitation,[44] which can be applied in bioimaging.

One may further deduce the number distribution of the NV centers in the particles from the modulation depth histogram.

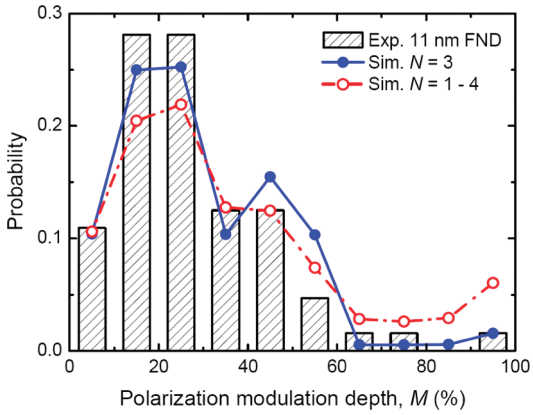

Figure 8. Experimental and simulated histograms of the fluorescence modulation depths of 11 nm FND particles. The experimental result was obtained for 64 particles. The blue dot line is the simulated distribution with three NV centers only, and the red dot−dash line is a linear combination of the simulated distribution with one, two, three, and four NV centers. The corresponding weighting factor is chosen according to the antibunching results reported in ref 37.

The blue dot line in Figure 8 is the simulated distribution with three NV centers only, and the red dot line is a linear combination of the simulated distribution with one, two, three, and four NV centers. The corresponding weighting factor is chosen according to the antibunching results previously reported.[37] As noted, most particles (more than 40% of the total population) have three centers. With this number of NV centers in an 11 nm FND particle, the average separation between the fluorophores is ~6 nm. This separation is too large to allow fluorescence resonance energy transfer to occur.[37,45]

Finally, it should be emphasized that the method developed in this work is not limited to quantifying the number of NV centers in FNDs only. It is general and applicable to other nanoparticles, polymers, and molecular complexes containing multiple and randomly orientated fluorophores as well.[35] Because the PMS technique requires only $\sim 10^5$ photons for detection, which takes about 10 s to measure one single FND particle, we can accomplish a modulation depth histogram (like the one shown in Figure 8) readily with a scanning confocal fluorescence microscope in 1 h. Compared to PCS, which usually requires 10^6-10^7 photons per measurement, PMS clearly provides a rapid alternative to obtain the average number (and, possibly, the number distribution) of NV centers in the FND particles. Thanks to the significant reduction of photons (more than 10-fold), the technique can estimate the number of fluorophores at the single-molecule level without the worry of photobleaching.[46]

CONCLUSION

We have developed a PMS technique to quantify the average number of fluorophores in nanoparticles at the single-molecule level. We take account of the heterogeneous dipole orientation and simulate the observed fluorescence modulation depths by Monte Carlo calculations. Tested with single FNDs with a mean size of 11 nm, our experiments show that these particles can contain an average number of 3 ± 1 NV centers, which is in good agreement with independent PCS measurements. Compared with PCS, PMS is advantageous because it does not demand two photodetectors and fast electronics in the quantification. The technique is simple and rapid, allowing measurements to be completed within a reasonably short period of time.

ASSOCIATED CONTENT

Supporting Information. Derivation of eqs 3 and 4. This material is available free of charge via the Internet at http://pubs.acs.org.

AUTHOR INFORMATION

Corresponding Author

*E-mail: yyhui@pub.iams.sinica.edu.tw (Y.Y.H.); hcchang@po.iams.sinica.edu.tw (H.-C.C.).

ACKNOWLEDGMENT

This work is supported by Academia Sinica and the National Science Council, Taiwan, with Grant No. 99-2119-M-001-026. T.-S.L. acknowledges the financial support from National Science Council with Grant No. NSC 99-2112-M-029-006-MY3.

REFERENCES

(1) Kitson, S. C.; Jonsson, P.; Rarity, J. G.; Tapster, P. R. *Phys. Rev. A* **1998**, *58*, 620–627.
(2) Weston, K. D.; Dyck, M.; Tinnefeld, P.; Müller, C.; Herten, D. P.; Saue, M. *Anal. Chem.* **2002**, *74*, 5342–4349.
(3) Fore, S.; Laurence, T. A.; Yeh, Y.; Balhorn, R.; Hollars, C. W.; Cosman, M.; Huser, T. *IEEE J. Sel. Top. Quantum Electron.* **2005**, *11*, 873–880.
(4) Rabeau, J. R.; Stacey, A.; Rabeau, A.; Prawer, S.; Jelezko, F.; Mirza, I.; Wrachtrup, J. *Nano Lett.* **2007**, *7*, 3433–3437.
(5) Bradac, C; Torsten, G.; Naidoo, N.; Rabeau, J. R.; Barnard, A. S. *Nano Lett.* **2009**, *9*, 3555–3564.
(6) Hui, Y. Y.; Chang, Y.-R.; Lim, T.-S.; Lee, H.-Y.; Fann, W.; Chang, H.-C. *Appl. Phys. Lett.* **2009**, *94*, 013104.
(7) Ha, T.; Enderle, T.; Chemla, D. S.; Selvin, P. R.; Weiss, S. *Phys. Rev. Lett.* **1996**, *77*, 3979–3982.
(8) Hu, D.; Yu, J.; Wong, K.; Bagchi, B.; Rossky, P. J.; Barbara, P. F. *Nature* **2000**, *405*, 1030–1033.
(9) Tinnefeld, P.; Weston, K. D.; Vosch, T.; Cotlet, M.; Weil, T.; Hofkens, J.; Mullen, K.; De Schryver, F. C.; Sauer, M. *J. Am. Chem. Soc.* **2002**, *124*, 14310–14311.
(10) Latychevskaia, T. Y.; Renn, A.; Wild, U. P. *J. Lumin.* **2006**, *118*, 111–122.
(11) Wei, P.-K.; Lin, Y.-F.; Fann, W.; Lee, Y.-Z.; Chen, S.-A. *Phys. Rev. B* **2001**, *63*, 045417.
(12) Sun, W.-Y.; Yang, S.-C.; White, J. D.; Hsu, J.-H.; Peng, K.-Y.; Chen, S. A; Fann, W. *Macromolecules* **2005**, *38*, 2966–2973.
(13) Lim, T.-S.; Hsiang, J.-C.; White, J. D.; Hsu, J.-H.; Fan, Y.-L.; Lin, K.-F.; Fann, W. *Phys. Rev. B* **2007**, *75*, 165204.
(14) Wu, E.; Jacquesa, V.; Treussarta, F.; Zeng, H.; Grangier, P.; Roch, J.-F. *J. Lumin.* **2006**, *119−120*, 19–23.
(15) Schietinger, S.; Barth, M.; Aichele, T.; Benson, O. *Nano Lett.* **2009**, *9*, 1694–1698.
(16) Zheng, D. Ph.D. Thesis, Ecole Normale Supérieure de Cachan, 2010.
(17) Vaijayanthimala, V.; Chang, H.-C. *Nanomedicine* **2009**, *4*, 47–55.
(18) Xing, Y.; Dai, L. *Nanomedicine* **2009**, *4*, 207–218.
(19) Fu, C.-C.; Lee, H.-Y.; Chen, K.; Lim, T.-S.; Wu, H.-Y.; Lin, P.-K.; Wei, P.-K.; Tsao, P.-H.; Chang, H.-C.; Fann, W. *Proc. Natl. Acad. Sci. U.S.A.* **2007**, *104*, 727–732.
(20) Neugart, F.; Zappe, A.; Jelezko, F.; Tietz, C.; Boudou, J.-P.; Krueger, A.; Wrachtrup, J. *Nano Lett.* **2007**, *7*, 3588–3591.

(21) Faklaris, O.; Garrot, D.; Joshi, V.; Druon, F.; Boudou, J.-P.; Sauvage, T.; Georges, P.; Curmi, P. A.; Treussart, F. *Small* **2008**, *4*, 2236–2239.
(22) Hui, Y. Y.; Cheng, C.-L.; Chang, H.-C. *J. Phys. D: Appl. Phys.* **2010**, *43*, 374021.
(23) Jelezko, F.; Wrachtrup, J. *Phys. Status Solidi* **2006**, *203*, 3207–3225.
(24) Epstein, R. J.; Mendoza, F. M.; Kato, Y. K.; Awschalom, D. D. *Nature Phys.* **2005**, *94*, 94–98.
(25) Davies, G.; Hamer, M. F. *Proc. R. Soc. London, Ser. A* **1976**, *348*, 285–298.
(26) Mayer Alegre, T. P.; Santori, C.; Medeiros-Ribeiro, G.; Beausoleil, R. G. *Phys. Rev. B* **2007**, *76*, 165205.
(27) Rand, S. C. In *Properties and Growth of Diamond*; Davies, G., Ed.; EMIS Datareviews Series; INSPEC; The Institute of Electrical Engineers: London, 1994; Vol. 9, Chapter 7.4.
(28) Gruber, A.; Drabenstedt, A.; Tietz, C.; Fleury, L.; Wrachtrup, J. *Science* **1997**, *276*, 2012–2014.
(29) Kurtsiefer, C.; Mayer, S.; Zarda, P.; Weinfurter, H. *Phys. Rev. Lett.* **2000**, *85*, 290–293.
(30) Dutt, M. V; Childress, L.; Jiang, L.; Togan, E.; Maze, J.; Jelezko, F.; Zibrov, A. S.; Hemmer, P. R.; Lukin, M. D. *Science* **2007**, *316*, 1312–1316.
(31) Balasubramanian, G.; Chan, I. Y.; Kolesov, R.; Al-Hmoud, M.; Tisler, J.; Shin, C.; Kim, C.; Wojcik, A.; Hemmer, P. R.; Krueger, A.; Hanke, T.; Leitenstorfer, A.; Bratschitsch, R.; Jelezko, F.; Wrachtrup, J. *Nature* **2008**, *455*, 648–651.
(32) Taylor, J. M.; Cappellaro, P.; Childress, L.; Jiang, L.; Budker, D.; Hemmer, P. R.; Yacoby, A.; Walsworth, R.; Lukin, M. D. *Nat. Phys.* **2008**, *4*, 810–816.
(33) Rittweger, E.; Han, K. Y.; Irvine, S. E.; Eggeling, C.; Hell, S. W. *Nat. Photonics* **2009**, *3*, 144–147.
(34) Goldstein, H. *Classical Mechanics*, 2nd ed.; Addison-Wesley: Reading, MA, 1980.
(35) Fraaije, J. G. E.; Kleijn, J. M.; van der Graaf, M.; Dijt, J. C. *Biophys. J.* **1990**, *57*, 965–975.
(36) Lai, N. D.; Zheng, D.; Jelezko, F.; Treussart, F.; Roch, J.-F. *Appl. Phys. Lett.* **2009**, *95*, 133101.
(37) Mohan, N.; Tzeng, Y.-K.; Yang, L.; Chen, Y.-Y.; Hui, Y. Y.; Fang, C.-Y.; Chang, H.-C. *Adv. Mater.* **2010**, *22*, 843–847.
(38) Chang, Y.-R.; Lee, H.-Y.; Chen, K.; Chang, C.-C.; Tsai, D.-S.; Fu, C.-C.; Lim, T.-S.; Tzeng, Y.-K.; Fang, C.-Y.; Han, C.-C.; Chang, H.-C.; Fann, W. *Nat. Nanotechnol.* **2008**, *3*, 284–288.
(39) Rondin, L.; Dantelle, G.; Slablab, A.; Treussart, F.; Bergonzo, P.; Perruchas, S.; Gacoin, T.; Chang, H.-C.; Jacques, V.; Roch, J.-F. *Phys. Rev. B* **2010**, *82*, 115449.
(40) Walker, J. *Rep. Prog. Phys.* **1979**, *42*, 1605–1659.
(41) Davies, G. *J. Phys. C* **1979**, *12*, 2551–2566.
(42) Zyubin, A. S.; Mebel, A. M.; Hayashi, M.; Chang, H.-C.; Lin, S. H. *J. Comput. Chem.* **2009**, *30*, 119–131.
(43) Tisler, J.; Balasubramanian, G.; Naydenov, B.; Kolesov, R.; Grotz, B.; Reuter, R.; Boudou, J.-P.; Curmi, P. A.; Sennour, M.; Thorel, A.; Börsch, M.; Aulenbacher, K.; Erdmann, R.; Hemmer, P. R.; Jelezko, F.; Wrachtrup, J. *ACS Nano* **2009**, *3*, 1959–1965.
(44) Faklaris, O.; Garrot, D.; Joshi, V.; Boudou, J.-P.; Sauvage, T.; Curmi, P. A.; Treussart, F. *J. Eur. Opt. Soc. Rapid Pub.* **2009**, *4*, 09035.
(45) Van der Meer, B. W.; Coker, G.; Chen, S.-Y. S. *Resonance Energy Transfer: Theory and Data*; VCH Publishers: New York, 1994.
(46) Ha, T. *Methods* **2001**, *25*, 78–86.